Research report

SCC tests for thermally cycled specimens and metallographic characterization

Ahmed Mazhar, Risto Ilola, Iikka Virkkunen

1 Introduction

This technical report presents the research done within the TOFFEE project WP3, Thermally induced stress corrosion cracking at Aalto University. The research in TOFFEE WP3 focuses on investigation of the role of thermal loads in promoting SCC.

2 Experimental

2.1 Test material and sample manufacturing

Two rings of 150 mm in length of austenitic 316L stainless steel pipe (diameter 326 mm, thickness 33 mm, Figure 1) were received from VTT. The material represents the material used in OL3 primary cooling circuit. Chemical composition of the pipe material is presented in Table 1.

The 150 mm long pipe rings were welded together at Suisto Engineering with NG-GTAW method using 316LSi filler metal (Table 1). The welding was done according to a WPS received from TVO, so that the weld represents the OL3 primary circuits welds.

Table 1. Chemical composition of the pipe material and filler metal.

	C	Mn	Si	P	S	Cr	Ni	Mo	Cu	N
Base material	0.028	1.81	0.39	0.022	0.002	17.1	12.03	2.27	0.56	0.08
Filler metal	0.02	1.8	0.85	0.023	0.002	18.3	11.4	2.5	0.2	0.073

Three segments of 140 mm x 65 mm in size were sawed from the welded pipe for SCC tests in autoclaves at VTT. Prior to the SCC tests, a selected location at the weld root in the weld segments were thermally cycled by heating them up to peak temperature in 4 s and cooling them down to room temperature in 30 s. Induction heating and air cooling were used and the cycles was repeated for three times. Three different peak temperatures were applied: 300, 400 and 500 °C, respectively.

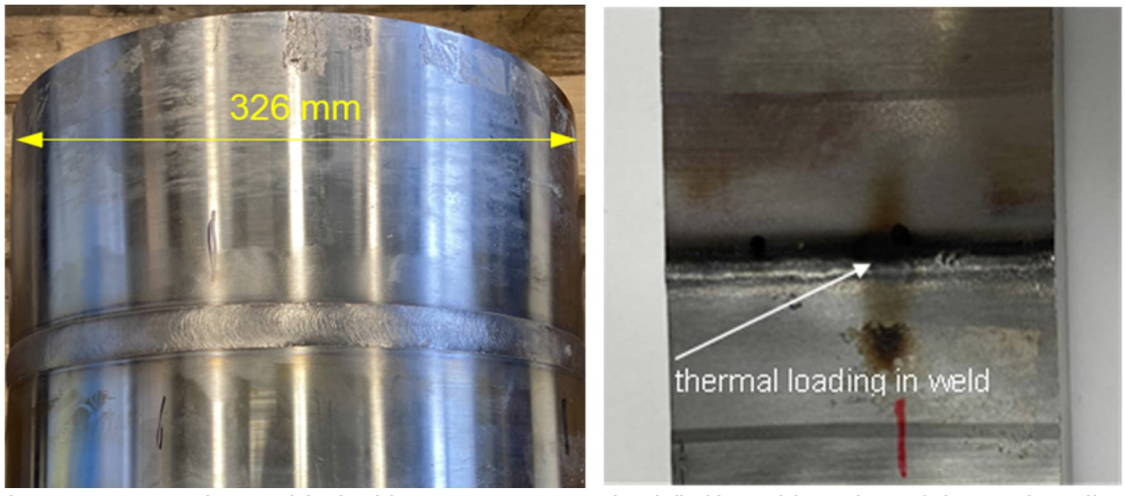

Figure 1. 316L pipe welded with NG-GTAW method (left) and location of thermal cycling on the inner surface of the pipe (right).

Thermal loading at peak temperature of 500 °C produced maximum axial tensile residual stresses of order of 500 MPa at close to the weld fusion line. At peak temperatures of 300 and 400 °C, the maximum residual stresses were about 250 and 100 MPa, respectively. Tensile residual stresses in non-thermally cycled locations were considerably lower. The hoop residual stresses were

generally lower at the thermally cycled locations, but in the non-thermally cycled locations there was anomaly in the results. The variation in the residual stress values can be considered typical to residual stress measurements.

2.2 Metallography and hardness testing

A metallographic sample of the weld cross-section was prepared for measurement of the weld hardness profile and metallographic investigation. The sample was ground and polished mechanically. Etching was performed electrochemically in a 60% HNO_3 + 40 % H_2O solution using 3 V current. Hardness profile was measured from three locations in the weld cross-section (Figure 2) using a HV1 scale (1 kg load). The distance between the measurement points was 1 mm.

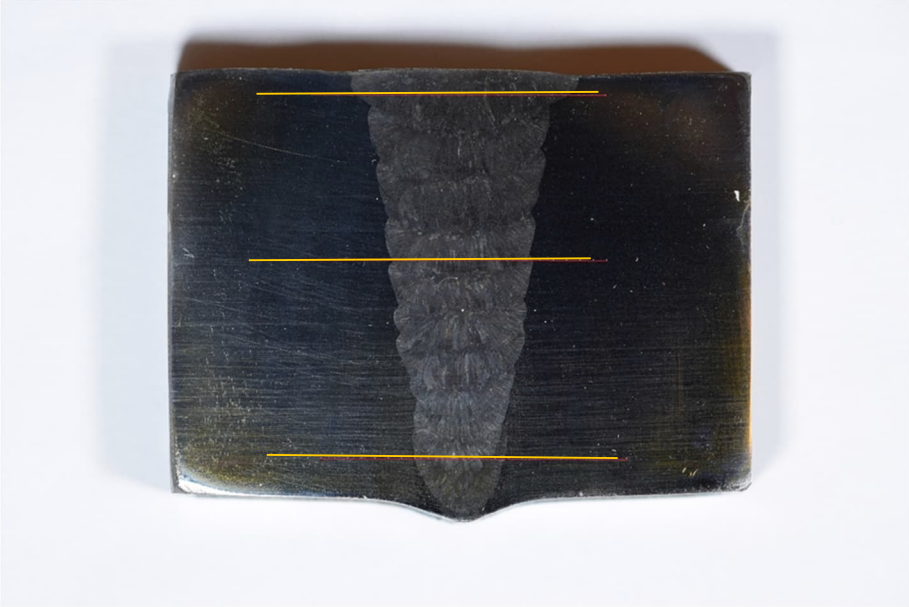

Figure 2. Location of hardness measurement lines in the pipe weld cross-section.

2.3 SCC tests

Susceptibility of the thermally cycled samples to SCC was carried out in autoclaves. The test parameters are presented in Table 2.

Table 2. Test parameters in the SCC tests.

Testing Parameters	Values
Hydrogen water chemistry	25 cc/kg
Temperature	325 °C
Pressure	140 bar
Exposure time	4 weeks
External loading	No
Sample condition monitored during testing	No

2.4 SEM analysis

After the autoclave exposure tests, the samples were examined in as-polished condition by optical microscopy and SEM to find out possible appearance of SCC. SEM-EBSD analysis was carried out on the sample to observe the non-uniformity of microstructure, crystallographic orientation, phase distribution and misorientation within the grains. The microstructure of the weld was also studied in as-etched condition.

3 Results

3.1 Hardness measurements

Hardness profiles measured from three different locations of the weld cross-section before the autoclave exposure tests are presented in Figure 3. Hardness values were the greatest in the weld root location being of order of 250 HV1 at maximum. The lowest hardness values were measured on the bead side of the weld. The hardness of the base material was below 200 HV1, which is typical for the pipe material in solution annealed and quenched condition.

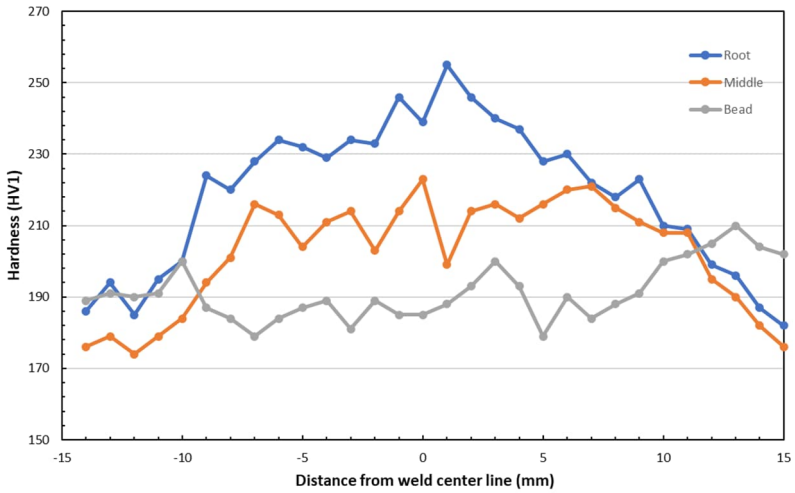

Figure 3. Hardness profile of the weld measured from the root side, bead, and middle of the weld.

Table 3. Hardness values (HV1) in the different positions of the weld cross-section and location of the measurement (BM = base material, W =weld).

Distance from weld centre line (mm)	Root	Point location	Middle	Point location	Bead	Point location
-14	186	BM	176	BM	189	BM
-13	194	BM	179	BM	191	BM
-12	185	BM	174	BM	190	BM
-11	195	BM	179	BM	191	BM
-10	200	BM	184	BM	200	BM
-9	224	BM	194	BM	187	BM
-8	220	BM	201	BM	184	BM
-7	228	BM	216	BM	179	BM
-6	234	BM	213	BM	184	W
-5	232	BM	204	BM	187	W
-4	229	BM	211	W	189	W
-3	234	BM	214	W	181	W
-2	233	W	203	W	189	W
-1	246	W	214	W	185	W
0	239	W	223	W	185	W
1	255	W	199	W	188	W
2	246	W	214	W	193	W
3	240	W	216	W	200	W
4	237	BM	212	W	193	W
5	228	BM	216	W	179	W
6	230	BM	220	W	190	W
7	222	BM	221	BM	184	W
8	218	BM	215	BM	188	BM
9	223	BM	211	BM	191	BM
10	210	BM	208	BM	200	BM
11	209	BM	208	BM	202	BM
12	199	BM	195	BM	205	BM
13	196	BM	190	BM	210	BM
14	187	BM	182	BM	204	BM
15	182	BM	176	BM	202	BM

3.2 Optical microscopy

Macrostructure of the weld cross-section is presented in Figure 4. The weld consists of 13 welding runs.

Figure 4. Cross-section of the studied AISI 316 NG-GTAW weld (pipe thickness 33 mm).

Microstructures of the base material and weld are presented in Figures 5 - 11.

Figure 5. Austenitic microstructure of the base material, average grain size G = 6 (scale bar 100 µm).

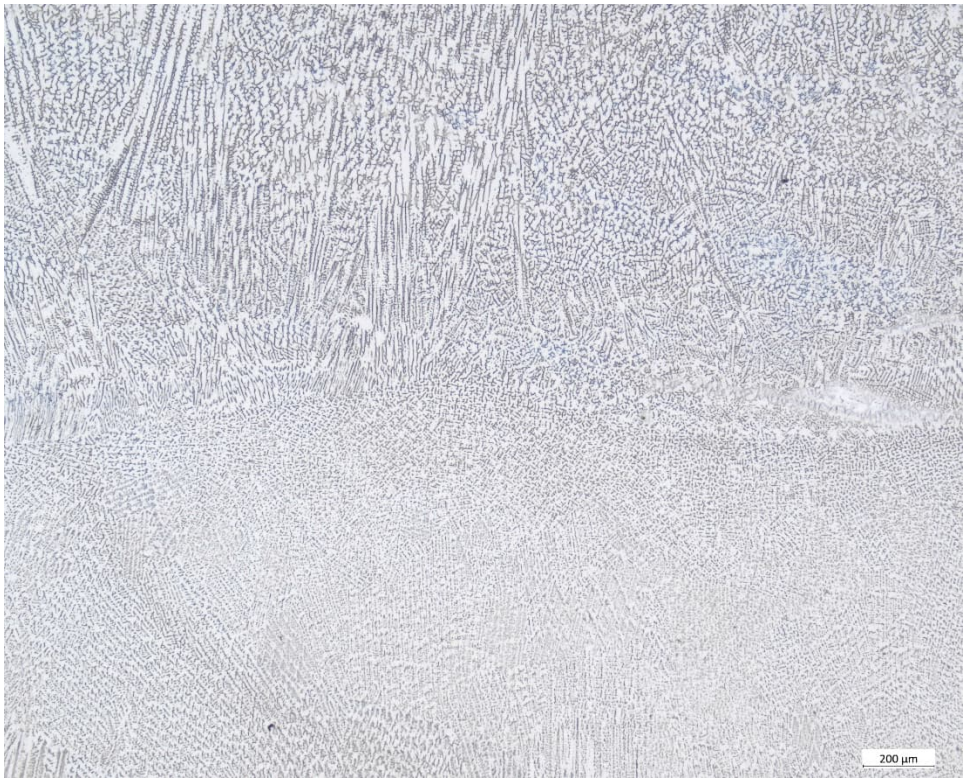

Figure 6. Austenitic weld structure and delta ferrite (scale bar 200 µm).

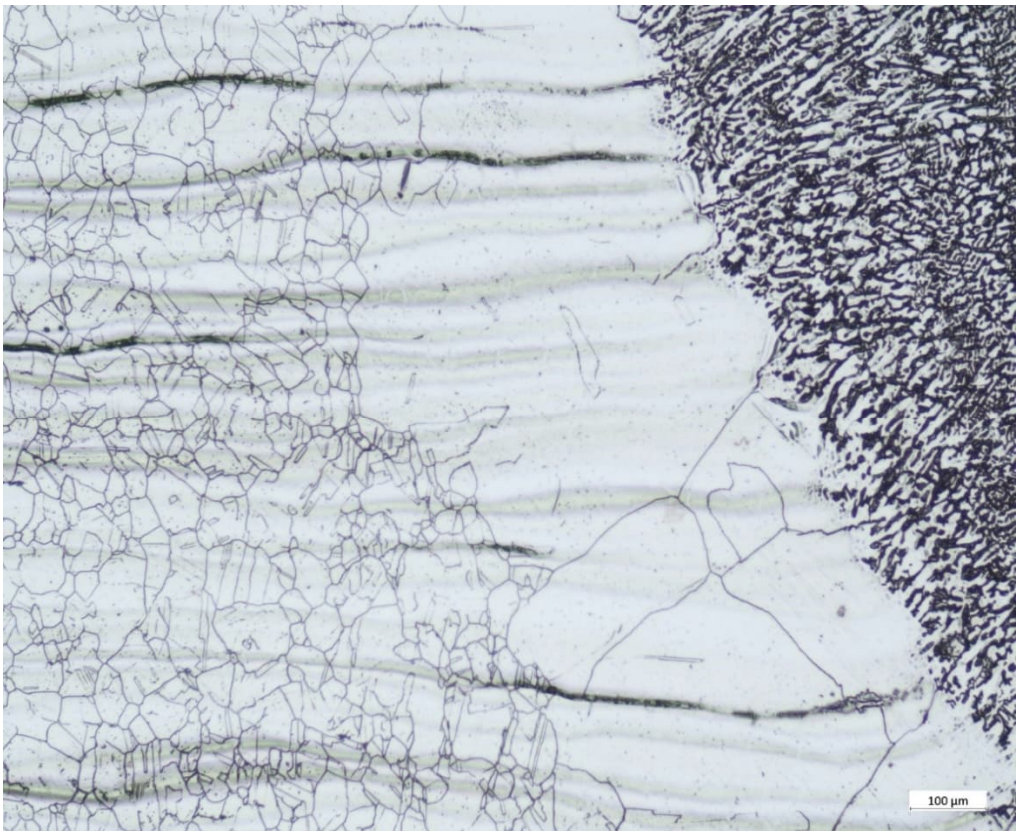

Figure 7. HAZ microstructure at the weld root showing coarse grain zone, and deformation in the base material (scale bar 100 µm).

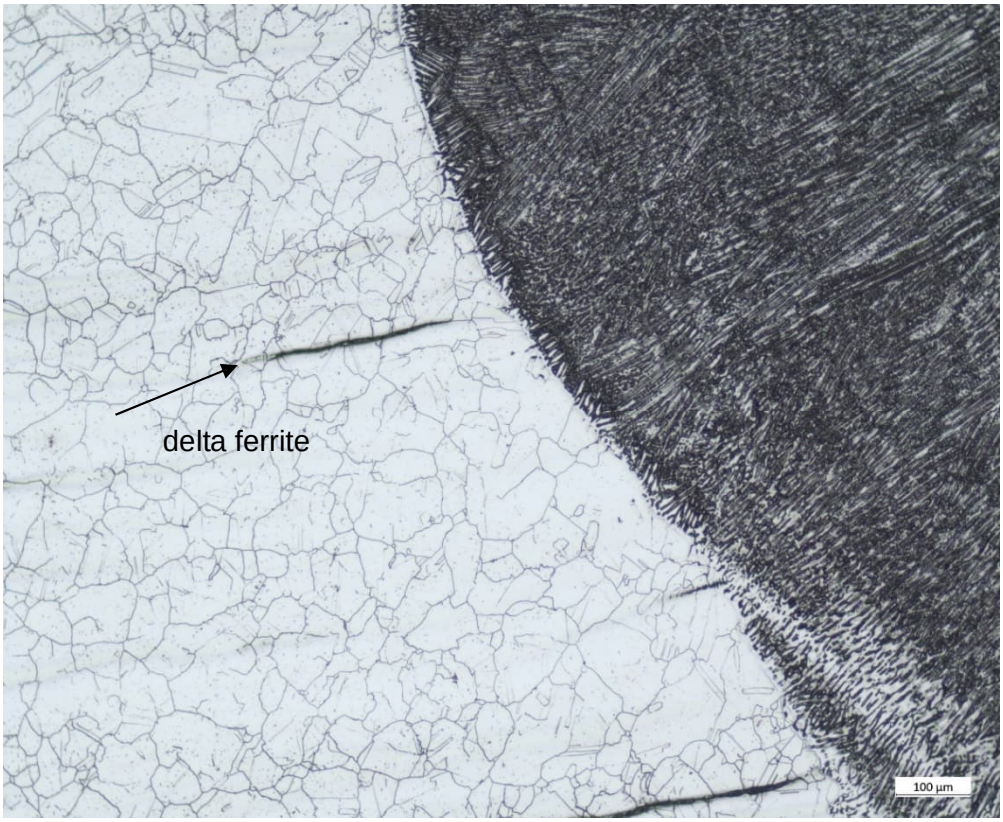

Figure 8. Microstructure in middle of the pipe cross-section having lamellar delta ferrite stringers close to the fusion line (scale bar 100 µm).

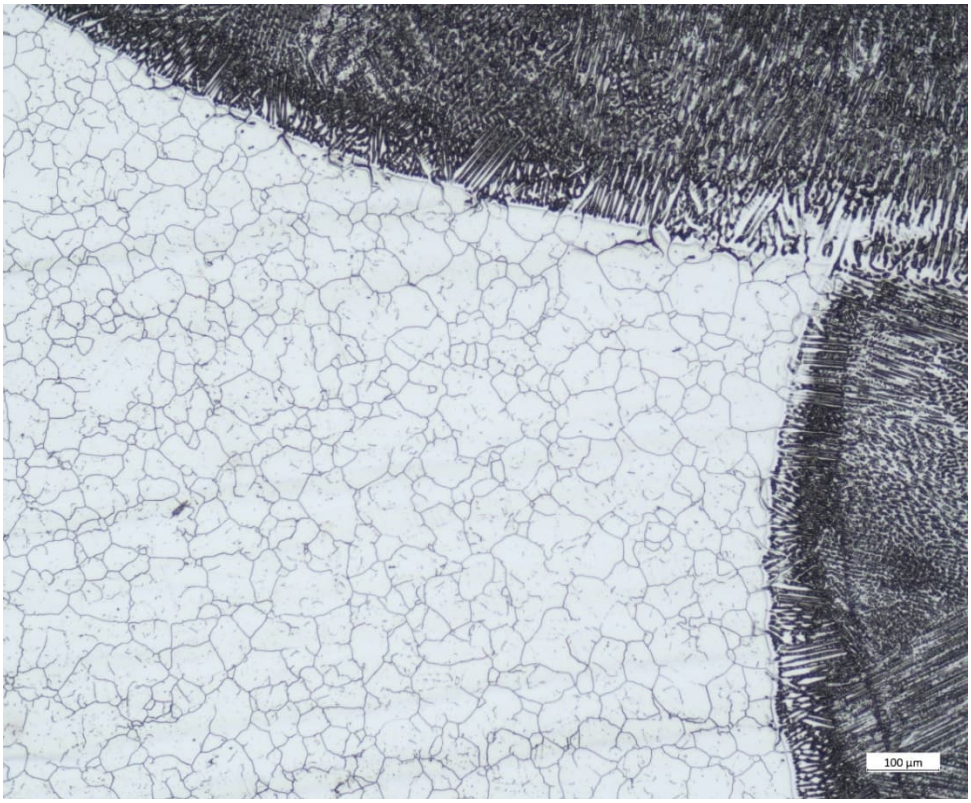

Figure 9. Microstructure at the upper part of the pipe cross-section presenting the HAZ and columnar weld solidification structure at the fusion line (scale bar 100 µm).

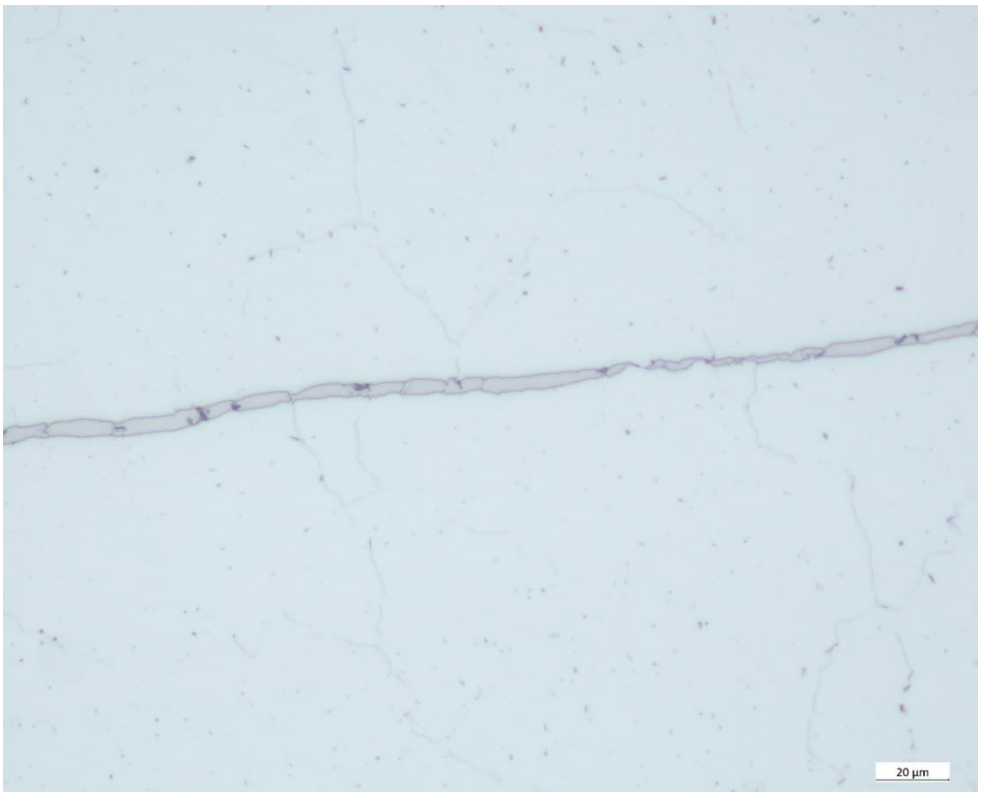

Figure 10. A lamellar delta ferrite stringer in the base material (scale bar 100 µm).

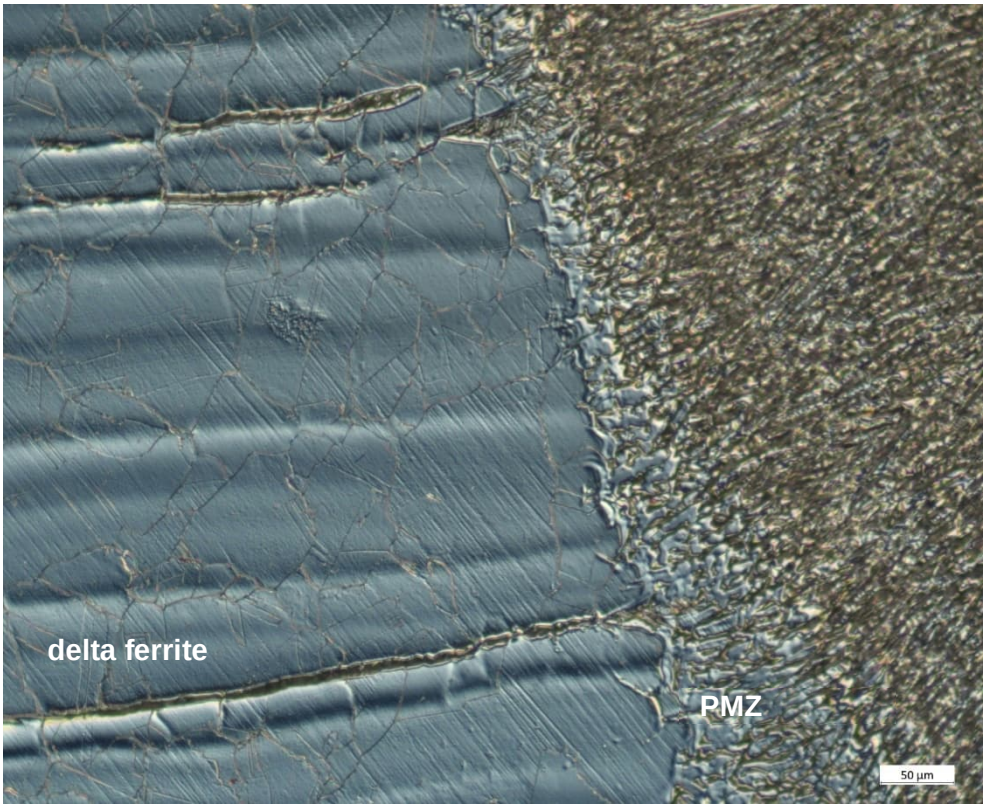

Figure 11. Delta ferrite stringers in the base material and PMZ (partially melted zone), DIC image (scale bar 50 μm.

The base material microstructure was typical to solution annealed austenitic steel (Fig. 5) having some individual elongated delta ferrite stringers (Fig. 10). The measured average grain size number G was 6. The orientation of delta ferrite was along the direction of deformation formed in pipe manufacturing (Fig. 15). In the weld, the delta ferrite was not elongated, and it was distributed uniformly. Columnar weld solidification that was perpendicular to fusion line was observed (Figs. 9 and 11). Only in the vicinity of the weld root, a HAZ region zone was seen (Fig. 7).

3.3 SEM-EBSD investigation

SEM investigation was performed for the sample that was thermally cycled at 500 °C and subjected to autoclave exposure test for 4 weeks. After the autoclave test, there were no detectable cracks in the microstructure, although the surface residual stress values were of order of 500 MPa in the sample after welding and thermal cycling. This was against the expectations.

IPF orientation maps

IPF (inverse pole figure) maps represent the crystallographic orientation of grains in polycrystalline materials. The IPF color codes show which crystal direction is parallel to sample surface normal direction. The IPF orientation maps from two locations in the weld are shown in Figure 12.

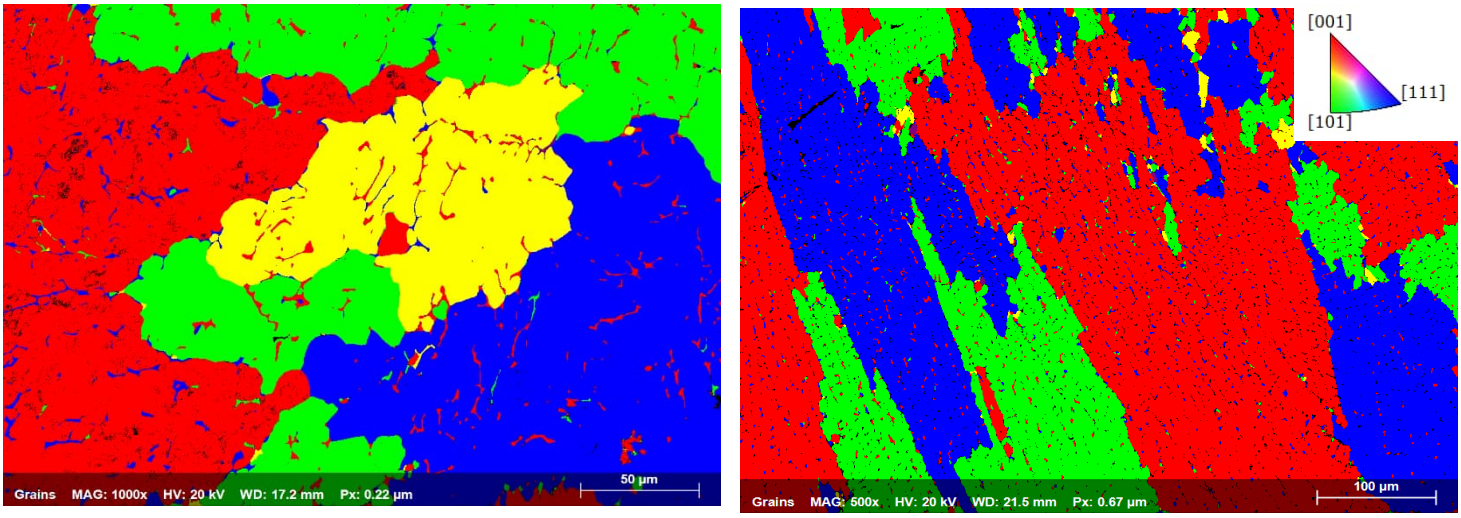

Figure 12. EBSD-IPF maps from two locations in the weld showing variation in the morphology of the grain structure. The structure is mainly austenite having some amount of delta ferrite.

The figures show variation of grain morphology due to welding and some amount of delta ferrite within the austenitic weld structure. The base material microstructure was a typical equiaxed microstructure of a solution annealed austenitic steel (Fig. 13).

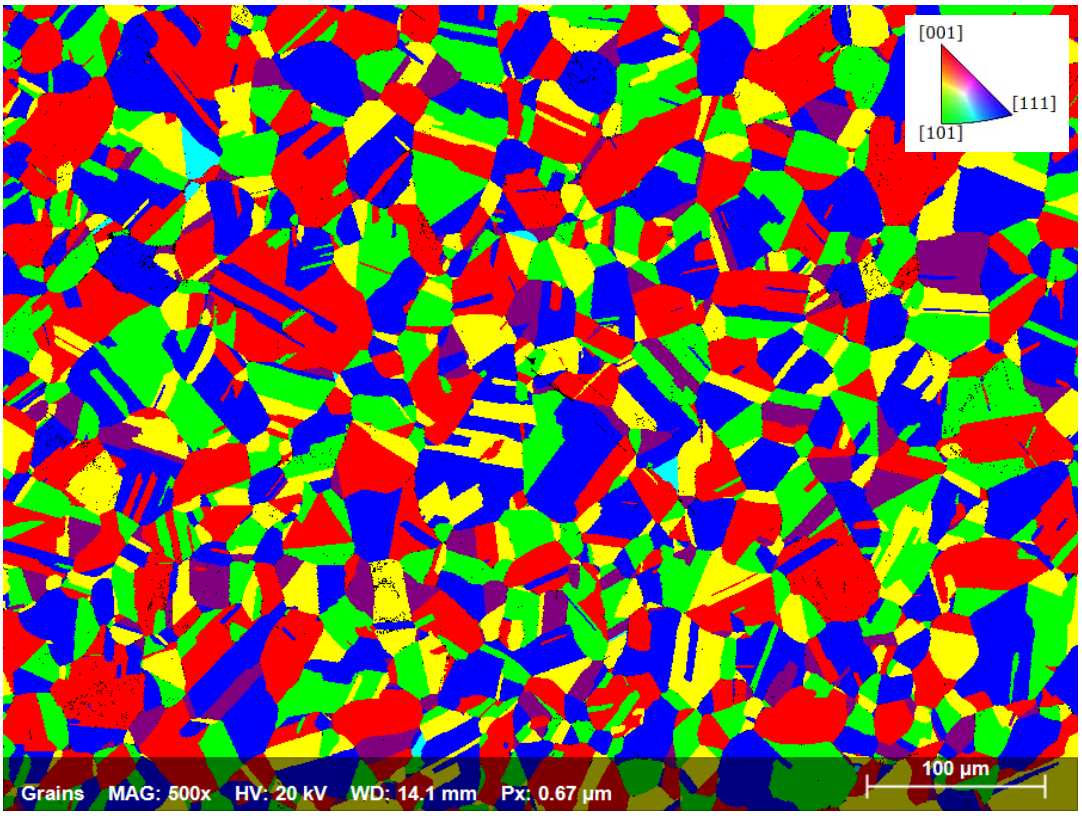

Figure 13. EBSD-IPF orientation map for the base metal shows an equiaxed austenite grains.

Phase maps

The second phase found in optical microscopy was identified as delta ferrite in SEM-EBSD phase mapping in weld (Figure 14) and base material (Figure 15). The delta ferrite content in the analysed region was 4 %.

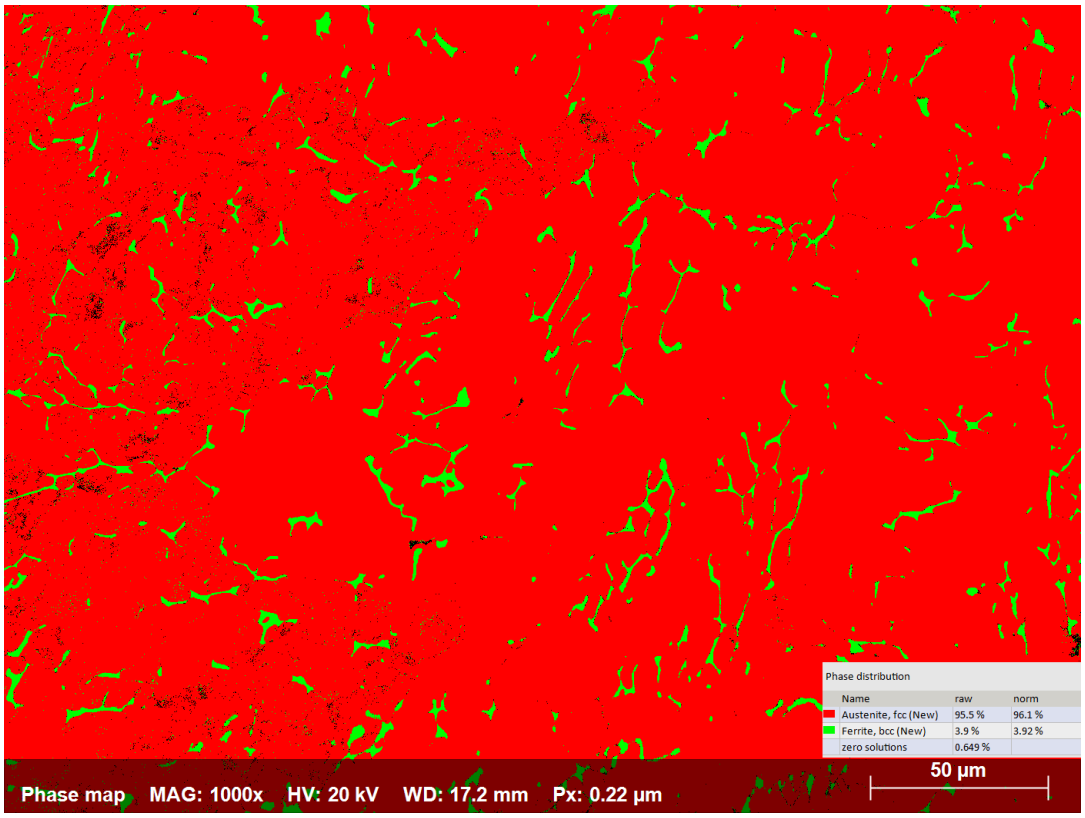

Figure 14: Phase map taken from the weld showing 96% austenite and 4% delta ferrite.

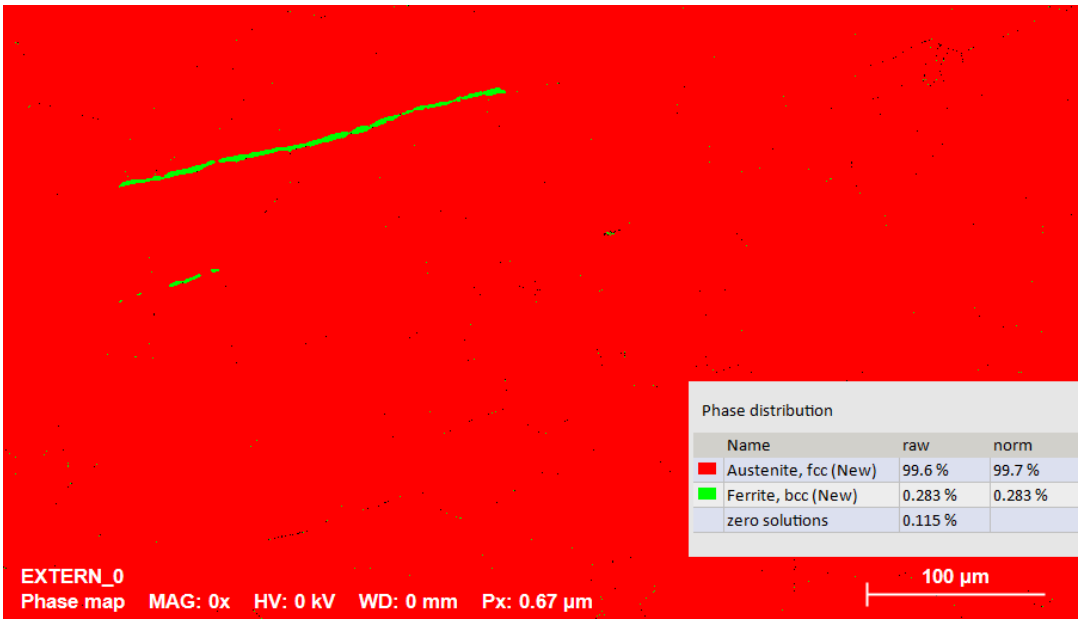

Figure 15. Phase map taken from the base metal showing delta ferrite stringers within austenite.

Average MO maps

EBSD average MO (misorientation) maps are used to visualize potential stress accumulation and stress concentration in the material. They represent overall distortion within the studied region. The MO average map measured from the weld and base metal from the root side close to the surface are presented in Figures 16 and 17, respectively.

The average MO maps show that there are areas (green, yellow and red) of high misorientation in both the weld and base metal. In the weld, they are due to welding and thermal cycling, but in the base material they are probably due to pipe surface machining before welding and pipe manufacturing. The blue areas in the figures indicate little or no strain accumulation.

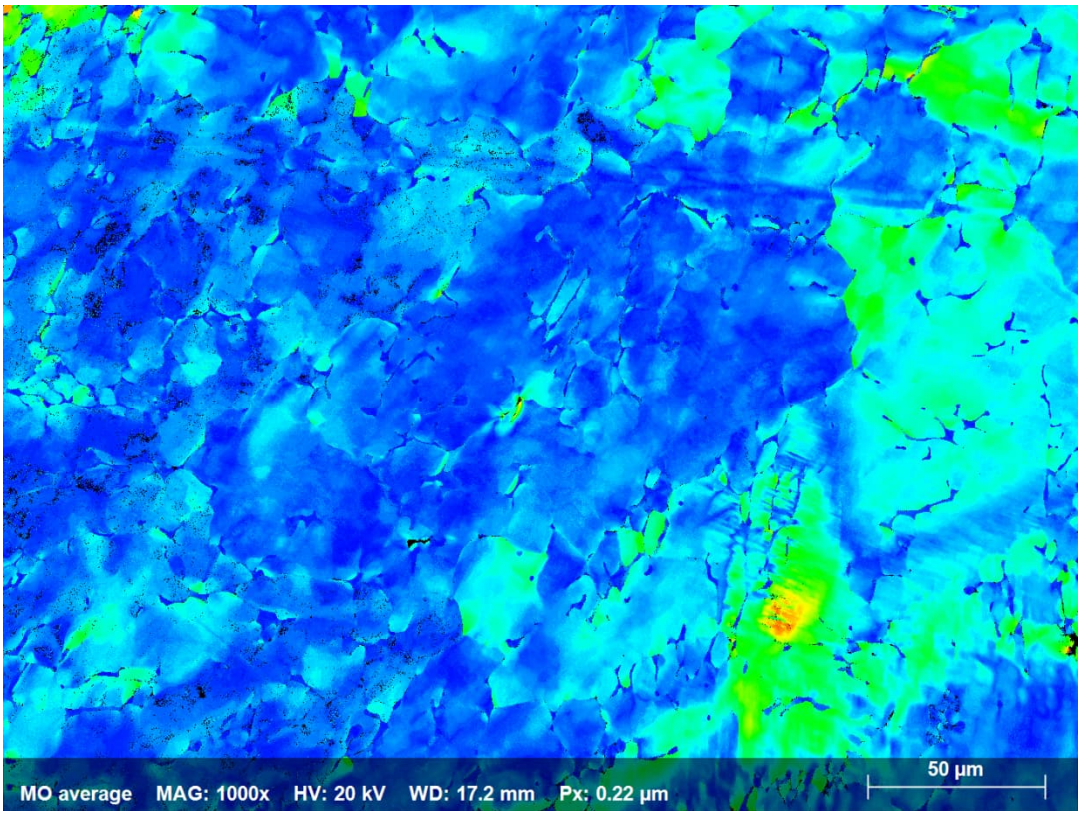

Figure 16. MO average map of weld metal indicating local areas (green, yellow, red) of high amount of deformation.

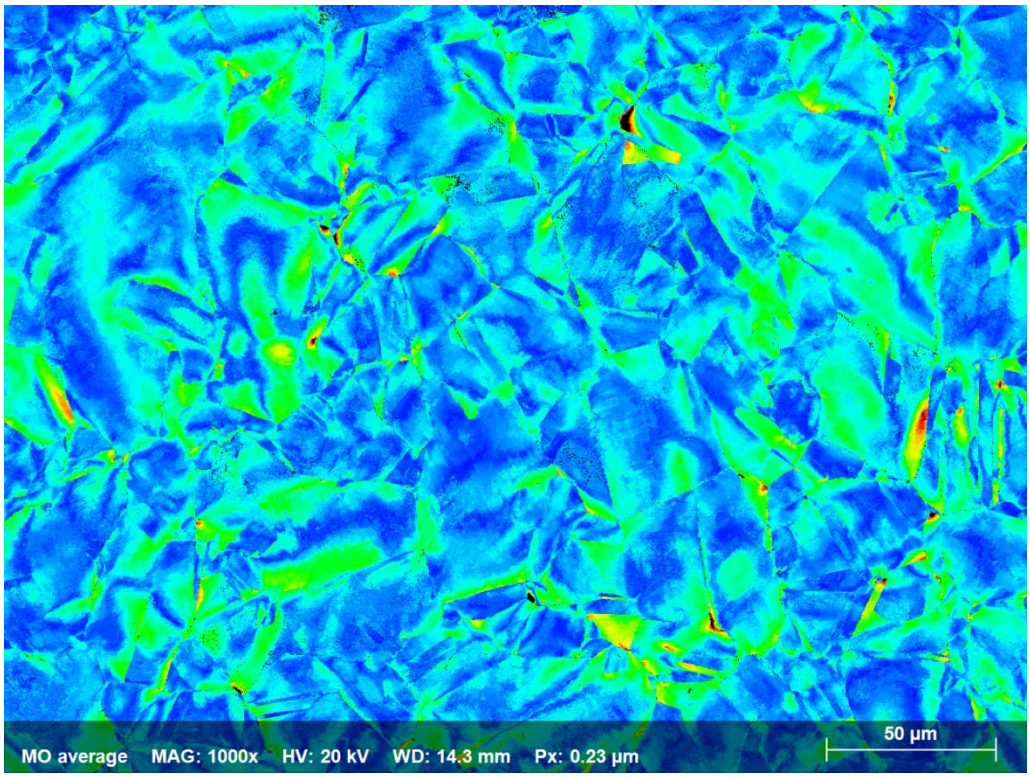

Figure 17. EBSD average MO map taken from the base metal pipe inner surface close to weld root.

4 Conclusions

Thermally cycled weld specimens having maximum tensile residual stresses of order of 500 MPa were tested in autoclaves and analyzed. Despite of the high stresses after welding and thermal cycling, no cracking was observed after 4 weeks autoclave exposure tests. Indications of stress concentrations in the vicinity of the weld root was observed in SEM-EBSD average MO maps, but they were not sufficient to cause cracking. Occurrence of SCC could have required constant loading during the autoclave tests.

Microstructural studies showed that the base metal was in solution annealed condition and that the hardness values were clearly greater in the weld than in the base metal. Optical microscopy and SEM showed only individual delta ferrite stringers in the base metal, but in the weld, the delta ferrite was clearly present. Grain size in HAZ close to the weld root was clearly greater than in the other HAZ locations.